



Effect of Ultrasonic Shot Peening on Oxidation Behavior of T91 and SS347 Steels in Air and Steam at 650 °C

Deepsovan Mondal, Kausik Chattopadhyay, and Vakil Singh

(Submitted September 18, 2019; in revised form May 9, 2020; published online August 28, 2020)

Ultrasonic shot peening (USP) is a relatively new process of surface modification to improve mechanical properties as well as corrosion and high-temperature oxidation resistance of metallic materials. The effect of USP on surface properties and the process of high-temperature oxidation in air and steam environment, following USP of the T91 and SS347 steels, was studied in this investigation. Surface modification by USP was done on the T91 and SS347 steels for different time periods of 0.5, 1.0, 1.5, 2.0 and 3.0 min. Microstructural modification, increase in surface roughness and enhancement in microhardness up to a depth of 300–350 μm were observed due to USP. There was also increment in surface roughness as well as microhardness with USP time duration. Thermogravimetric analysis of the oxidation tests showed parabolic oxidation kinetics at 650 °C for both the steels. Comparatively more protective oxide scales, containing high amount of Cr, were formed on the USP-treated samples. The thickness of the oxide scale was reduced with increase in the USP time duration. Oxidation resistance of the T91 steel at 650 °C, both in air and steam, was improved by the USP treatment. Oxidation resistance of the SS347 steel at 650 °C was also improved for the USP2.0 and the USP3.0 conditions.

Keywords SS347 steel, T91 steel, air oxidation, steam oxidation, ultrasonic shot peening

1. Introduction

Increasing environmental awareness all over the world is driving the economy toward reduction of CO₂ emissions and less fuel consumption in supercritical power plants by increasing power generation efficiency. For conventional fossil fuel power plant, efficiency is a strong function of temperature and pressure of steam entering the turbine (Ref 1, 2). Research and development of heat-resistant steels and alloys for highly efficient supercritical power plants at 650 °C and above are now being promoted (Ref 2). Alloys used at high temperature should possess combination of good mechanical properties, corrosion and oxidation resistance. However, in the normal ferritic steel, oxidation resistance derives from the formation of Cr containing oxides, which become less protective at higher temperatures in both steam and exhaust environments (Ref 3–5).

In recent years, various chromium-molybdenum ferritic heat-resistant steels have been developed for use as main steam pipes or super-heater tubes in power generation boiler because of their high strength over a wide range of temperature (Ref 6). 9Cr-1Mo ferritic-martensitic steel is widely used in thermal power plants as a thick steam pipe component for heat exchanger, steam super-heater and re-heater applications (Ref 1, 2, 6–10). It possesses good heat transfer properties, adequate

mechanical properties, resistance against low cycle fatigue, creep and oxidation under steam and furnace gases over the operating temperature range of 550 to 650 °C (Ref 5, 6). Niobium and vanadium are added to modified 9Cr-1Mo steel (ASME T91) to improve its high-temperature mechanical properties (Ref 6–8). However, this steel suffers from oxidation and hot corrosion from long time exposure in severe environment or at higher temperature (Ref 1–5, 9–11). It is well known that adhesion of the oxide scales is a very important factor for oxidation resistance of a material. Detachment of oxide scale causing impact damage and downstream blockage resulting in overheating has proved to be a serious problem in super-heater tubes (Ref 12). Type SS347 is a high-carbon, columbium (niobium)- and tantalum-stabilized austenitic chromium-nickel stainless steel, found suitable for applications demanding high-temperature resistance against fall in mechanical properties and environmental degradation (Ref 2, 13, 14). SS347 steel shows good strength and oxidation resistance up to 680 °C due to higher amount of Cr and Ni (Ref 13). It also contains niobium (Nb) and tantalum (Ta) as stabilizing elements to maximize its creep strength and resistance against inter-granular corrosion (Ref 14). This steel is used in higher temperature region of heat exchanger, super-heater and in some critical parts of super-heater along with the T91 steel welded together (Ref 15, 16).

Recently, many researchers have paid much attention to nanocrystalline materials because of their superior mechanical, physical and chemical properties (Ref 17, 18). Surface modification by nanocrystallization at surface is an alternative method for improving corrosion resistance of materials (Ref 17–20). The surface nanocrystallization can be obtained by several processes like ultrasonic shot peening (USP), laser shock peening (LSP), equi-channel angular pressing (ECAP), high pressure torsion (HPT), etc. The enhanced electrochemical behavior of the refined grains at surface was attributed to increase in density of diffusion paths available for alloying elements, which migrate rapidly and form a protective passive film (Ref 18, 20). Therefore, surface nanocrystallization would

Deepsovan Mondal, Kausik Chattopadhyay, and Vakil Singh, Department of Metallurgical Engineering, Indian Institute of Technology (BHU), Varanasi 221005, India. Contact e-mail: kausik.met@iitbhu.ac.in.

result in early formation of passive film with enhanced corrosion as well as oxidation resistance.

Ultrasonic shot peening (USP) is a technique in which hard balls of steel, ceramic or glass bead with high sphericity, impact surface of the material at high frequency (Ref 21, 22). A vibrating surface called sonotrode directly in contact with the peening shots is used to transmit the kinetic energy to shots. Firstly, a generator produces a sinusoidal electric signal that excites a piezo-electric transducer, which converts the electric energy into a mechanical displacement. Since the vibration delivered by the transducer is small, the vibration is amplified by a series of boosters and enough kinetic energy is transferred to sonotrode (Ref 21). The frequency of vibration is within the ultrasonic wave range (20 kHz), which explains the name of the technique and the amplitude of vibration kept in a range of 40–80 μm . Typical ball sizes are 1–3 mm in diameter; however, they could also be of larger size (Ref 22). During the impact, each piece of impinging shot acts as a tiny peening hammer generating small indentation or dimple by plastically deforming the surface due to which hardness and surface roughness alter. Compressive residual stresses are generated at the USP-treated surface as heavy plastic deformation occurs on the surface due to impact of the shots and fatigue life of materials is improved (Ref 23–25). Additionally, USP process protects the material against penetration of undesirable gases and liquids through removal of porosities (Ref 24). On the other hand, corrosion and oxidation resistance of alloys can also be improved through refinement of grains in surface region by USP (Ref 25–29). Due to multiple random impacts of shots, severe plastic deformation occurs at the material surface and dislocation density of surface layers increases rapidly. As the material gets heated, the deformed surface region recrystallizes or forms a sub-grain boundary structure, which finally leads to development of ultra-fine grains in the surface region (Ref 25). These can affect the diffusion mechanisms of diffusive alloying elements and hence can change the oxidation kinetics of these alloys (Ref 25, 29). For different ferritic/martensitic and stainless steels, the enhanced diffusion of chromium ions along the large number of dislocations and grain boundaries generated by USP leads to early formation of the protective chromium-rich oxide layer, which slows down further growth of the iron oxide layer due to its low permeability for $\text{Fe}^{2+}/\text{Fe}^{3+}$ or O^{2-} through it (Ref 26–29).

The purpose of this study was to investigate the high-temperature oxidation behavior of the T91 and the SS347 steels in air and steam environment after surface modification through USP treatment.

2. Experimental Procedure

2.1 Material

All the experiments in this investigation were carried out on the modified 9Cr-1Mo (ASME T91 grade) ferritic/martensitic steel and austenitic stainless steel SS347, provided by the Coastal Gujarat Power Limited (CGPL), TATA Power, Mundra, India. These steels were provided in form of tube with outer diameter of 42.2 mm and thickness of 7.3 mm. The chemical compositions of the above tube materials were determined using optical emission spectrometer (OES) and are presented in Table 1. The USP, air oxidation and steam oxidation tests were

carried out using disk-shaped samples of 12 mm diameter and 5 mm thickness. These samples were prepared from the supplied tubes, cutting into ring and subsequently into small pieces and machining on lathe. These specimens were mechanically polished on emery papers of 1000, 1500 and 2000 grit size using rotating polishing wheel. Prior to test, the samples were cleaned in an ultrasonic cleaner using acetone, at room temperature for 4 min, to remove sticking particles from the surface, if any.

2.2 Ultrasonic Shot Peening

USP was carried out by Stress Voyager (SONATS) using 100C6 grade hardened steel balls of 3 mm diameter and 665VHN hardness, at a constant amplitude of 80 μm and frequency of 20 kHz for different durations of 0.5, 1.0, 1.5, 2.0 and 3.0 min. The as-polished un-shot peened samples are designated as Un-USP and the samples subjected to USP for 0.5, 1.0, 1.5, 2.0 and 3.0 min are designated as USP0.5, USP1.0, USP1.5, USP2.0 and USP3.0 respectively.

The shot peened specimens were sectioned into two halves, perpendicular to USP treated surface, using a diamond-coated circular saw, to characterize microstructural modifications in the surface region caused by the USP and to evaluate variation of microhardness from USPed surface to interior. Before microstructural observation and microhardness test, the cross-sectioned surfaces were polished on emery papers of 1000, 1500 and 2000 grit size and subsequently on velvet cloth using alumina powder as abrasive, on rotating polishing wheel.

2.3 Hardness Measurement

The bulk hardness of the as-received T91 and SS347 steels was measured on polished surfaces of the disk specimens using Vickers Hardness testing machine Leco LV700AT at 500 gf load for 10 s dwell time. The variation of microhardness along the depth from the surface of the USP-treated samples was measured on the polished cross-sectioned surface, from the USP treated edge to inside, at 50 gf load for 10 s dwell time.

2.4 Surface Roughness Measurement

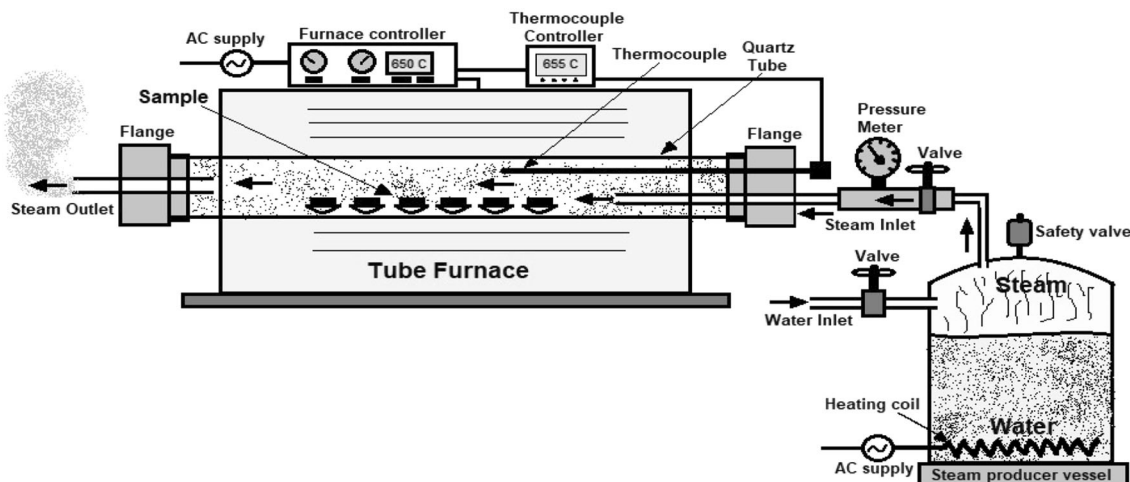
Surface roughness of the mechanically polished Un-USP and USP treated samples was measured by Mitutoyo SJ-410 profile meter. Prior to measuring of roughness, the profile meter was calibrated using standard sample. The roughness of each sample was measured at four different locations, and the average value was taken as surface roughness of the samples.

2.5 Oxidation in Air

Cyclic oxidation tests were performed in air at 650 °C in a tube furnace on the Un-USP specimen and the specimens subjected to USP for different time durations of 0.5, 1.0, 1.5, 2.0, 3.0 min. Each sample was kept in individual silica crucible and was put in an electric resistance-heating tube furnace operating at 650 °C. Prior to oxidation test, the crucibles were preheated at 500 °C for 1 h to remove moisture and volatile contents. The specimens were subjected to several heating and cooling cycles of different times of exposure. For oxidation test of the T91 steel at 650 °C, initially each cycle was of 3 h for the first 7 cycles, subsequently the next 3 cycles were of 6 h each, and finally the last 2 cycles of 12 h; thus, total duration of oxidation was 63 h. For the SS347 steel, firstly each cycle was of 4 h for 4 cycles, then of 8 h for next 2 cycles, then of 12 h

Table 1 Chemical composition of the as-received T91 and SS347 steels procured from the OES (wt.%)

	C	Si	Mn	P	S	Cr	Mo	Ni	V	Nb	Ta	Fe
T91	0.105	0.289	0.380	< 0.003	< 0.005	9.06	0.928	0.042	0.214	0.0752	...	Bal.
SS347	0.0661	0.473	1.49	< 0.005	< 0.005	18.5	0.201	10.4	...	0.589	0.42	Bal.

**Fig. 1** Schematic diagram of the steam oxidation test setup

for the next cycle and finally of 24 h for the last cycle, and the total duration of exposure was 68 h. After each cycle, the samples were taken out from the furnace and cooled to room temperature for 20 min. The weight of specimens along with the respective crucibles was measured using a digital balance, before and after each cycle of exposure. In some cases, the oxide scale formed was found exfoliated from the surface, but remained in the respective crucibles; thus, the total weight gain along with the oxide scales was measured. XRD analysis of the oxide scales was carried out to determine the products formed. The oxidized samples were sectioned in two halves, perpendicular to exposed surface, and the cross sections were mechanically polished to observe microstructural changes, oxide layers, and also for SEM, EDS study.

2.6 Oxidation in Steam

Cyclic oxidation tests in steam environment were performed at 650 °C for the T91 and SS347 steels for total duration of 48 h for the Un-USP and USPed specimens. The specimens were subjected to 12 heating cycles of 4 h of exposure in each cycle in steam and cooling to room temperature after each cycle.

The steam oxidation experiments were performed in an experimental setup, especially designed in-house for this purpose. The layout of the experimental setup is schematically shown in Fig. 1. The setup consists of an electric resistance-heating tubular furnace with an additional arrangement of steam generation outside the furnace and flow of steam through the tube furnace. Quartz tube was used in the furnace to ensure better stability at higher temperature and during steam flow. A pressure cooker vessel was used for producing steam. The vessel was first filled with water using the water inlet valve, and steam was produced by heating water using an electric

resistance-heating coil inside the vessel; a Bourdon tube pressure gauge was installed to check the steam pressure inside the vessel. When the steam pressure reached 1 kg/cm² and also the furnace temperature reached 200 °C, the flow of steam through the tube was started and continued throughout the cycle of heating and cooling, maintaining the pressure at 1 kg/cm². The samples were kept in clean and preheated silica crucibles and were put inside the tubular furnace, when the furnace temperature reached 650 °C. An extra thermocouple was installed inside the tube for proper measurement of temperature inside the tube, just above the sample. After each cycle of 4 h, the steam flow was stopped and the samples along with the crucibles were taken out from the furnace. The samples were cooled to room temperature and were weighed along with the respective crucibles, using a digital balance machine of 1 mg sensitivity. The oxidized samples were characterized by optical microscopy, SEM and XRD analysis of the oxide scale.

2.7 Optical Microscopy

Optical microscopy was carried out of the different samples to examine the microstructural changes caused by USP and the oxidation tests. The specimens of the as-received T91 and SS347 steels, USP treated for different durations, transverse section of oxidized in air and steam, were examined under LEICA DM1750M optical microscope at different magnifications. Before optical microscopy, the specimens were mechanically polished on emery papers of 1000, 1500 and 2000 grit size and subsequently on velvet cloth mounted on rotating disk using alumina powder slurry as abrasive. Care had been taken while polishing the sectioned surfaces of the oxidized samples to prevent detachment of the oxide layers formed, which might lead to loss of microstructural features at the oxidized edge. Subsequently, etching was done with Vilella's reagent (1 g

picric acid, 5 ml conc. HCl and 100 ml ethanol) for the T91 steel and with Aqua regia (10 ml of conc. HNO₃, 30 ml conc. HCl) for the SS347 steel.

2.8 SEM and EDS Analysis

In order to examine the oxide layer and microstructural changes, following oxidation and hot corrosion, scanning electron microscope (SEM) (ZEISS 840A) operating at 30 kV was used. Specimens for SEM-EDS were prepared by sectioning the oxidized samples perpendicular to the oxidized face using a thin diamond-coated circular saw and subsequently mechanical polishing and etching was done of the sectioned surfaces. EDS analysis was also done on the oxide scale and cross-sectioned surface to examine the compositional changes resulting from the oxidation tests.

2.9 XRD Analysis

X-ray diffraction was carried out of the as-received T91 steel, SS347 steel, different USP-treated samples, oxide layer of the oxidized samples, using a 18 kW rotating anode Rigaku miniflex600 x-ray diffractometer using Cu-K_α radiation ($\lambda = 0.1542$ nm) with scan rate of 10°/min from $2\theta = 20^\circ$ to 100°. The samples for XRD were prepared from the as-received material, USPed specimens, oxidized specimens, and their dimension was 10 mm × 10 mm × 3 mm. The XRD data were analyzed with the help of ICDD database to determine the phase changes resulting from USP and the different products formed from the air oxidation and steam oxidation.

3. Results and Discussions

3.1 The T91 Steel Super-Heater Material

The optical micrograph of the T91 steel in the Un-USP condition consisted of ferritic structure with some amount of martensite, and mean intercept length of the ferrite grains was 15–20 μm , in line with the earlier reports (Ref 7, 8, 10, 25).

The average bulk hardness of the as-received T91 was measured as 216 ± 5 VHN. This high hardness is due to presence of carbide particles like M₂₆C₆ (Cr₂₆C₆) and MC (VC,

NbC) types, along the grain boundaries, which strengthen the material and retard grain growth at high temperature.

3.1.1 Effect of Ultrasonic Shot Peening on the T91 Steel. The variation of surface roughness of the T91 steel with USP time duration is presented in Table 2. It can be seen that surface roughness of the USP-treated specimens was higher than that of the Un-USP specimen. The roughness increases rapidly with increase in USP time duration up to 2 min; then, the rate of increment is reduced. The surface roughness increases because of impact of shots on the material surface and formation of dimples and craters on the surface.

The Vickers microhardness values of the USP-treated samples are also presented in Table 2. It can be seen that microhardness in surface region of the USP-treated samples is higher than that of the Un-USP sample. The hardness decreases with increase in distance from the USP-treated edge, and the depth of hardened region is increased with the USP time period. The USP process enhanced microhardness of the USP0.5 by 51% and that of USP3.0 by 72% at a depth of 50 μm from the USP-treated edge. This increase in microhardness is attributed to increase in dislocation density, grain refinement and compressive residual stresses due to severe plastic deformation resulting from USP.

The SEM micrographs of surface of the USP1.5 sample are shown in Fig. 2. Dimples and crater-like features may be seen on the USP-treated surface of the T91 steel in the low magnification SEM micrograph (Fig. 2a). These dimples were formed due to random impacts of shots on the material surface at various angles. The shapes of the dimples are non-uniform. Size of the dimples varies from 300 to 500 μm . At low magnification, bottom surfaces of the dimples appear smooth (Fig. 2b), but at higher magnification (Fig. 2c) some very fine microcracks of less than 1 μm in width and depth are seen on the surface; however, these superficial cracks are not detected at the edge in cross section (Fig. 2d) of the USP-treated sample. USP is a process of severe plastic deformation at high strain rate in the surface region and causes rapid work hardening. Depending on the condition of USP, some micron or submicron size cracks may develop on the USP-treated surface. However, the compressive residual stress in the surface region induced by USP restricts propagation of the cracks and enhances fatigue life of the material.

X-ray diffraction patterns of the Un-USP, USP 0.5 and USP1.5 T91 steel samples (Fig. 3) reveal that both Un-USP as well as USP-treated specimens have BCC crystal structure and

Table 2 Data of surface roughness and microhardness for different USP-treated T91 and SS347 steels

Material	Condition	Surface roughness: R_a , μm	Hardness at 50 μm depth, HV	Depth of hardened layer from USP surface, μm
T91	Un-USP	0.325 ± 0.1	216 ± 5	00
	USP0.5	1.729 ± 0.15	328 ± 5	300 ± 10
	USP1.0	2.275 ± 0.15	342 ± 5	320 ± 10
	USP1.5	2.524 ± 0.15	352 ± 5	350 ± 10
	USP2.0	2.885 ± 0.15	368 ± 5	380 ± 10
	USP3.0	2.912 ± 0.15	373 ± 5	400 ± 10
SS347	Un-USP	0.43 ± 0.1	220 ± 5	00
	USP0.5	1.51 ± 0.15	363 ± 5	210 ± 10
	USP1.0	1.96 ± 0.15	385 ± 5	240 ± 10
	USP1.5	2.23 ± 0.15	401 ± 5	270 ± 10
	USP2.0	2.28 ± 0.15	412 ± 5	300 ± 10
	USP3.0	2.31 ± 0.15	418 ± 5	300 ± 10

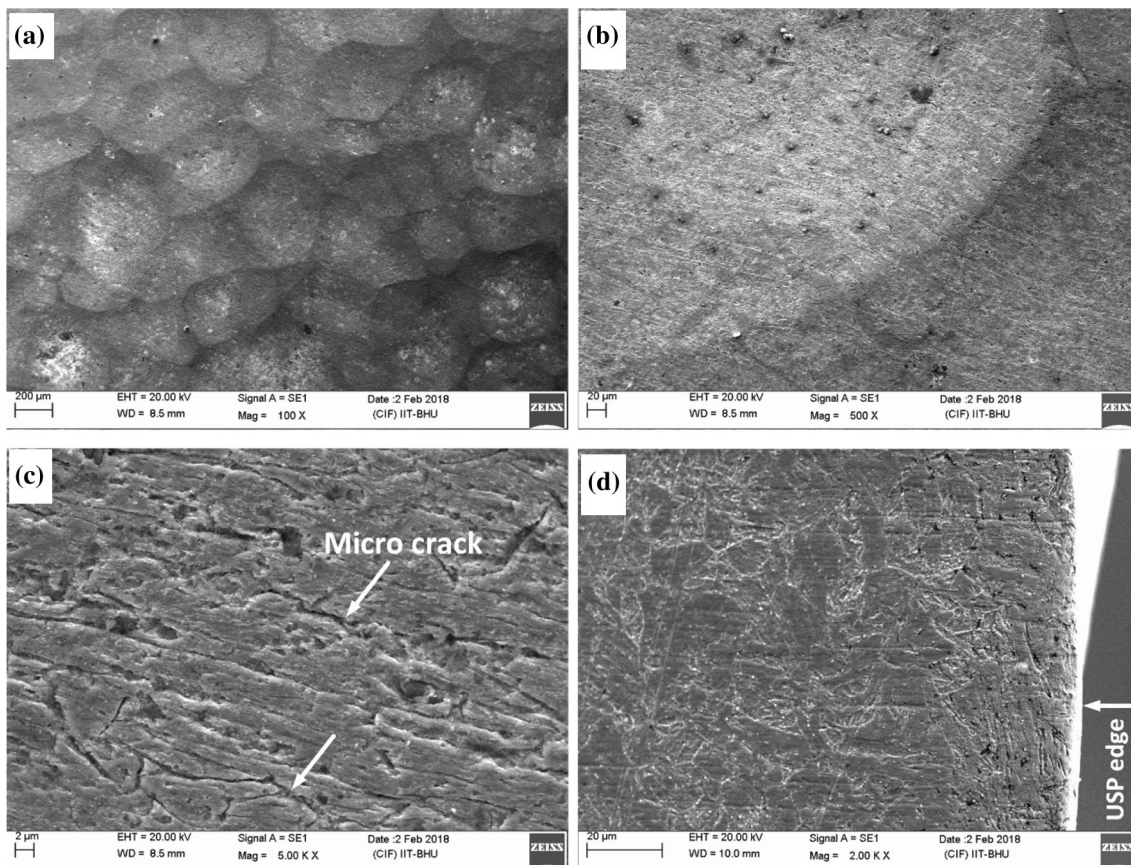


Fig. 2 SEM images of the T91 steel: (a)–(c) USP treated surface, (d) cross section image of USP1.5 sample

no phase transformation occurred due to USP. The Intensity of the (110) planes increased, and the intensities of the two other planes (200) and (211) decreased for the USP-treated samples than that of the Un-USP sample. The increase in the intensity of (110) peak in the USP-treated sample is due to increase in number of the planes in that orientation in the surface region. During severe plastic deformation, most of the planes try to accommodate themselves in a plane having lowest critical resolved shear stress, and the amount of reorientation of plane depends on the amount of shear strain (Ref 25, 30). As (110) is the highest atomic density plane and most preferred slip plane of BCC crystal structure, reorientation of most of the crystals occurred in that direction during USP, which led to (110) texture in surface region of the USP treated sample.

3.1.2 Oxidation of the T91 Steel in Air at 650 °C. The elementary stages of oxidation of a metal involve several fundamental steps, such as adsorption of gas molecules on the alloy surface, oxide nucleation and growth, oxygen dissolution, internal oxidation, formation of cavities and microcracks (Ref 1, 3-5, 11). According to Wagner's theory of oxidation, oxidation of metal progresses by ionic transportations of cations and anions through the oxide layer, and the rate of oxidation is controlled by partial ionic conductivities of oxides and their dependence on the chemical potential of the metal or oxygen in the oxide (Ref 31). The defect structure inside the oxide layers also plays an important role in oxidation. The most generalized form of the oxidation reaction is: $xM(s) + yO(g) = M_xO_y(s)$.

This reaction determines the amount of metal consumed, the amount of oxygen used and the amount of product formed

during oxidation process. There are several laws of oxidation that characterize the rate of oxidation such as linear, parabolic, cubic and logarithmic. If the total weight of the oxidizing material increases with the duration of oxidation, the oxidation rate is fitted mathematically using the equation: $(\Delta W)^n = K \cdot t$ where ' ΔW ' is weight gain per unit area in mg/cm^2 , ' K ' is a rate constant in $mg^n cm^{-2n} h^{-1}$ and ' t ' is exposure time in hour. From the above equation, another equation may be derived: $n \cdot \ln(\Delta W) = \ln(K) + \ln(t)$.

From the linear plot of ' $\ln(\Delta W)$ ' versus ' $\ln(t)$ ' the values of ' n ' and ' K ', characterizing oxidation kinetics are determined. Here ' n ' values of 1, 2 and 3 represent linear, parabolic and cubic oxidation kinetics, respectively. The linear law is followed when the surface reaction of metal with reactive gases of the environment is the dominating factor. The parabolic law is obeyed when diffusion through oxide scale is the main determining step. The logarithmic law, however, is applicable to very thin oxide films in the range of 20–40 nm (Ref 1, 3, 5). It has been observed previously that most of the iron-based high-temperature alloys exhibit parabolic kinetics of oxidation in the temperature range of 500–700 °C (Ref 1, 9–11, 26–29).

The variation of weight gain per unit area (ΔW) with exposure time for oxidation in air of the T91 steel at 650 °C for 63 h is shown in Fig. 4(a). It may be seen from Fig. 4(a) that the rate of weight gain during the initial 15 h of exposure was high and was reduced during the subsequent period of exposure up to 63 h. In general, the rate of weight gain was relatively lower for the USP-treated specimens in respect of the Un-USP specimen. The values of ' n ' were determined from the ' $\ln(\Delta W)$ ' versus ' $\ln(t)$ ' plot and are listed in Table 3. For most

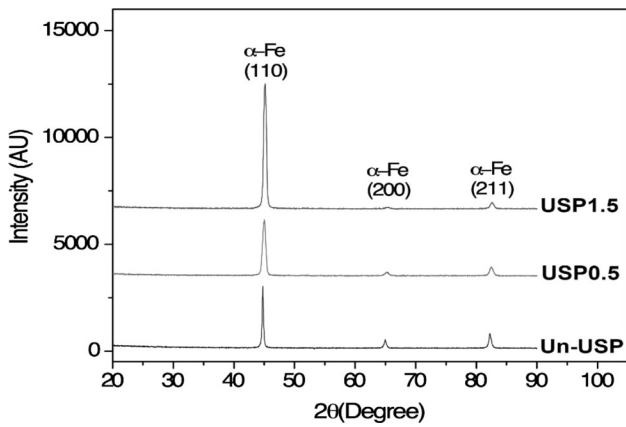


Fig. 3 XRD patterns of the Un-USP, USP0.5 and USP1.5 samples of the T91 steel

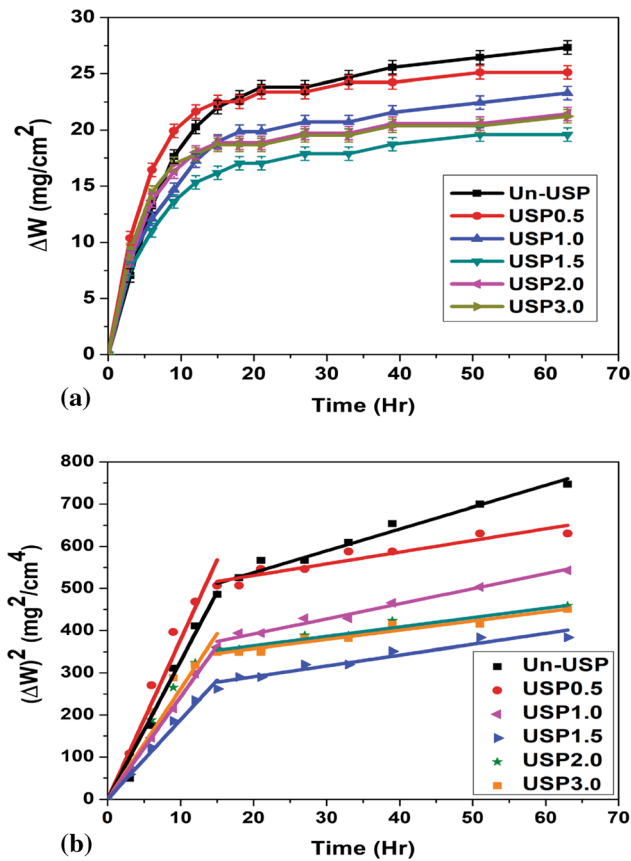


Fig. 4 Variation of (a) ΔW with exposure time, (b) $(\Delta W)^2$ with exposure time of different USP-treated T91 steel oxidized in air at 650 °C for 63 h

of the samples, the 'n' value was nearly 2 in the initial stage; thus, it was assumed that the oxidation kinetics followed parabolic rate law $(\Delta W)^2 = K_p \cdot t$, where ' K_p ' is parabolic rate constant. The plot of $(\Delta W)^2$ versus exposure time (Fig. 4b) was made and the values of ' K_p ' were determined from the linear segments of the plot, corresponding to the initial period of exposure up to 15 h and also for the later stage of exposure. For all the samples, the ' K_p ' values (Table 3) are very high for the initial stage and low for the later stage. The oxidation rate was

found to decrease for all the USP-treated specimens in respect of that of the Un-USP specimen. There was highest weight gain in the Un-USP sample and lowest in the USP1.5 sample.

The optical micrograph of cross sections of the T91 steel subjected to different USP durations, after 63 h of oxidation in air at 650 °C, shows a thick oxide layer over the surface (Fig. 5). The thickness of the oxide layer varied from 100 to 150 μm for the different samples. A clear oxide-substrate interface can be seen in the micrograph. A different region of 200-250 μm thickness can also be seen in the material at the oxide edge for the USP-treated samples, which may be the region modified by USP. Figure 6 shows SEM micrographs of the Un-USP and the USP1.5 T91 steel specimens after 63 h of oxidation in air at 650 °C. It is clearly seen that the oxide scale formed over the material surface is quite thick. For the Un-USP sample, the thickness of the layer is nearly 140-150 μm , whereas for the USP1.5 sample, it is 110-120 μm . In addition, the oxide layer is a double-layered structure, though there was no sharp interface between the two layers. The EDS analysis of cross section of the specimens oxidized in air for 63 h is also presented in Fig. 6, which shows that the outer layer of the oxide scale consists of mainly iron and oxygen, whereas the inner oxide consists of both iron and chromium. At a depth of 80-100 μm from the oxide surface, higher amount of Cr could be found at the inner oxide layer of the USP-treated sample than that of the Un-USP sample. Little amount of Mo and Mn was also present in oxide scale of the USP-treated sample. No chromium was found in the outer oxide layer of the Un-USP sample, but in case of the USP1.5 sample some amount of Cr was present at the outer scale also. The XRD patterns of the oxide scale formed after the oxidation in air for 63 h of the Un-USP and different USP-treated samples are shown in Fig. 7. All the patterns have almost same types of peaks at almost same positions as the oxide formed are of same type for all the samples; only the intensities of the peaks are different. All the oxide scales contain mainly Fe_2O_3 with some other minor compounds such as FeO , Cr_2O_3 and FeCr_2O_4 . It indicates that at the outer surface the most stable oxide formed is Fe_2O_3 . The intensity of any XRD peak depends on the amount of the related phase present in the oxide scale and also on the thickness of the oxide layer. For the Un-USP sample, the intensity of almost all the peaks are highest and for the USP1.5 sample the intensities are lowest. It means that the amount of Fe_2O_3 in the oxide scale, thickness of the oxide layer is highest in the Un-USP sample and are lowest in the USP1.5 sample.

During oxidation of ferrous alloy, a multi-layer scale consisting of Fe_2O_3 (hematite), Fe_3O_4 (magnetite) and some amount of FeO (wustite) forms at the surface (Ref 3, 5, 11). FeO is metal-rich oxide and requires lowest partial pressure of oxygen, whereas Fe_2O_3 is oxygen-rich oxide and requires a higher partial pressure of oxygen to form. The oxidation process in iron is mainly controlled by cation transport through wustite/magnetite and by anion diffusion through hematite (Ref 1, 3, 11). Though majority of the studies on high-temperature oxidation of steels are based on the assumption that oxides on steels grow only from outward diffusion of Fe, since the lattice diffusion coefficient of O anions in iron oxide is very small (Ref 9, 11, 27).

In Fe-Cr system, Cr has highest affinity to oxygen and can form an oxide at very low partial pressure of oxygen. Cr_2O_3 is the most stable oxide, which has the lowest ΔG of formation (Table 4) in this temperature range among the other oxides of Fe-Cr system; thus, it forms at the very initial stage of oxidation

Table 3 Data of rate constant of oxidation of Un-USP and different USP-treated T91 steel oxidized in air at 650 °C for 63 h

Sample	$n \ln(\Delta W) = \ln(K) + \ln(t)$		$(\Delta W)^2 = K_p t$			
	n	adj. R^2	Up to 15 h		After 15 h	
			$K_p, \text{mg}^2 \text{cm}^{-4} \text{h}^{-1}$	adj. R^2	$K_p, \text{mg}^2 \text{cm}^{-4} \text{h}^{-1}$	adj. R^2
Un-USP	1.39	0.97	32.76	0.992	5.17	0.961
USP0.5	2.04	0.96	37.86	0.985	2.78	0.887
USP1.0	2.09	0.99	24.27	0.999	3.58	0.976
USP1.5	2.21	0.98	18.85	0.994	2.56	0.913
USP2.0	2.02	0.96	26.08	0.988	2.22	0.930
USP3.0	2.30	0.94	26.18	0.988	2.18	0.935

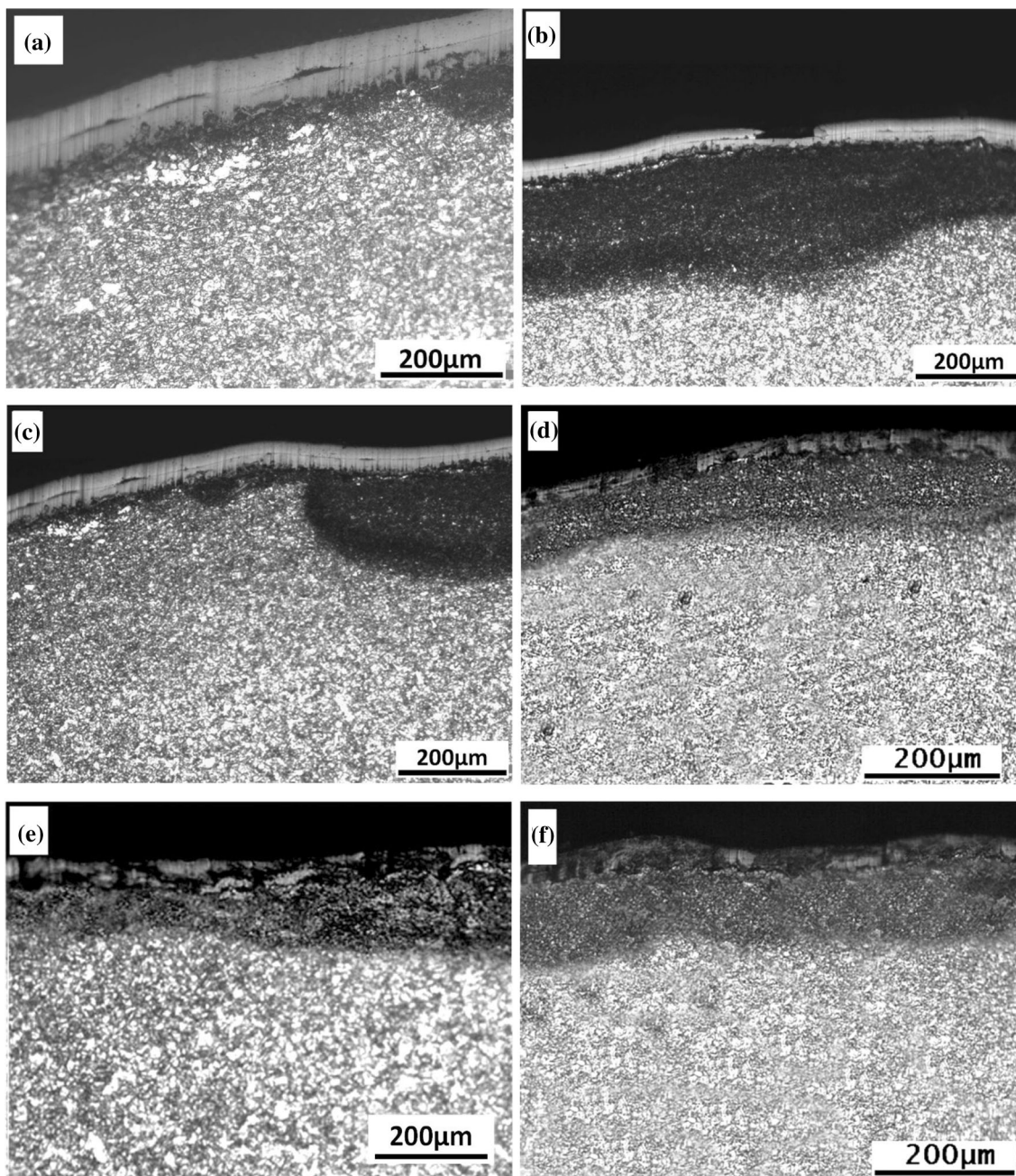


Fig. 5 Optical micrographs of the USP treated T91 steel oxidized in air at 650 °C for 63 h (a)Un-USP, (b) USP0.5, (c) USP1.0, (d) USP1.5, (e) USP2.0 and (f) USP3.0

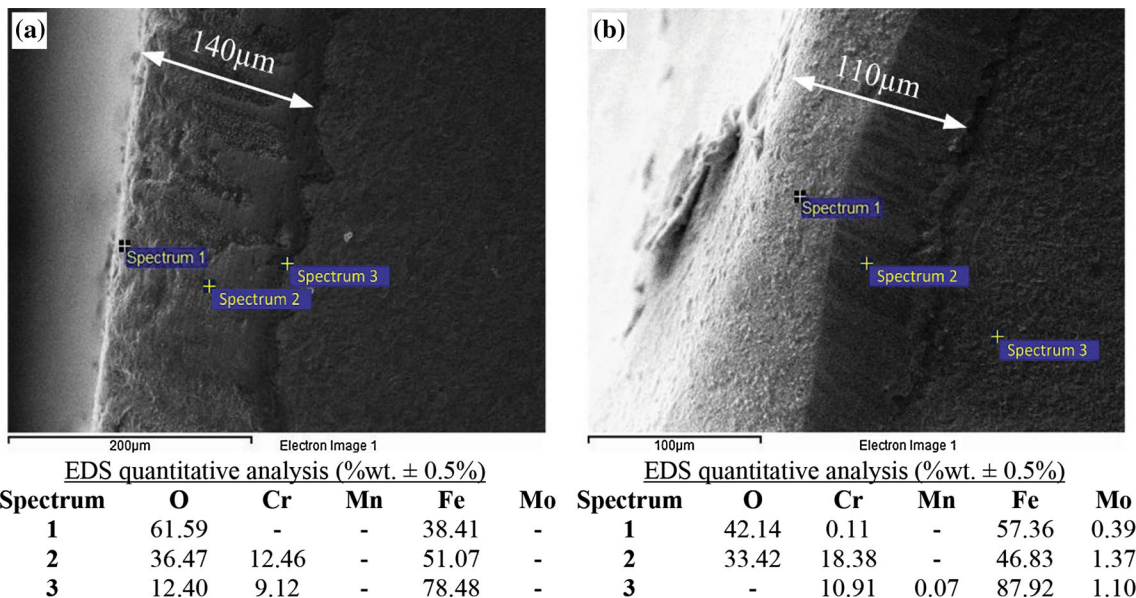


Fig. 6 SEM micrographs and EDS data of the (a) Un-USP, (b) USP1.5 T91 steel oxidized in air at 650 °C for 63 h

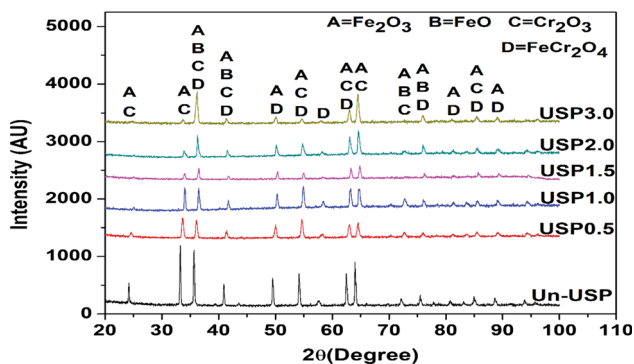


Fig. 7 XRD patterns of the Un-USP and USP treated T91 steel oxidized in air at 650 °C for 63 h

(Ref 5, 11, 32, 33). The formation of a continuous Cr_2O_3 scale over Fe-Cr alloys leads to decrease in the oxidation rate as the ionic diffusion coefficient through Cr_2O_3 is very low and it resists the transport of $\text{Fe}^{2+/3+}$ ions for the formation of iron oxide. It is well observed that steels containing higher amount of chromium show better oxidation resistance due to formation of more protective oxides; however, it is not clear that what is the minimum required amount of Cr in steel to efficiently develop a protective chromium oxide layer. Previous researches indicate that about 10-12 wt.% of Cr is borderline amount to form sufficiently protective Cr_2O_3 over the steel surface (Ref 1). In case of a steel having less than 12 wt.% Cr, the scale does not cover the whole surface therefore the surface is not fully protected from oxidation. At higher temperature or from long-time exposure, the subsequent depletion of Cr from the substrate, just below the oxide layer, lowers the Cr concentration at the alloy-scale interface. In such case, internal oxidation of the alloy occurs and iron enters the scale in large quantities. Fe and Cr, which were readily available at the oxidation front, oxidize to form a continuous oxide layer over the surface overlaid with iron-rich oxides due to internal oxidation effects. Cationic and anionic transportation occurs through the scale, causing outward growth of iron rich oxides. The outward

migration of Fe cations is promoted by the higher Fe concentration gradient created from the metal oxide to the oxide-gas interface. This leads to formation of an iron-rich oxide over the surface of the Cr-rich oxide layer, where the oxygen potential is also higher. Thus, Fe-Cr alloys containing less than 12 wt.% Cr produce scales which consist of outer layers of Fe_2O_3 and Fe_3O_4 and an inner layer whose composition is best described by $\text{Fe}_{(3-x)}\text{Cr}_x\text{O}_4$ (Ref 9-11, 27-29).

Because of USP, the process of diffusion of Cr and other alloying elements is modified. It is evident from the EDS analysis (Fig. 6) that the Cr, Mo, Mn content in the oxide scale was higher in the USP-treated specimen than that in the Un-USP specimen due to enhanced diffusion of the alloying elements. During heating in the initial hours, the dislocations introduced by USP served as fast-diffusion paths. The grain boundary area in the USP-affected region was marked increased due to extensive grain refinement by recrystallization or sub-grain formation. Earlier research has shown that 1-5 min of USP treatment resulted in grain refinement up to less than 1 μm in the surface region of T91 steel (Ref 25). Thus, enhanced diffusion of Cr through large number of grain boundaries in the USP-affected region to surface led to rapid formation of protective Cr_2O_3 layer at the surface. This acted as effective barrier for diffusion of oxygen to cause internal oxidation (Ref 27-29) and for outward diffusion of Fe. The EDS analysis also revealed less oxygen content in the oxide scale formed on the USP treated samples; it indicates that oxidation resistance of the USP-treated specimen was higher than that of the Un-USP specimens.

Initially, the rate of oxidation was high (Fig. 4b) since the unprotected bare material was directly in contact of the environmental oxygen at higher temperature. Fast reaction took place in this stage and stable oxides like Cr_2O_3 , Fe_2O_3 and Fe-Cr spinel started forming rapidly. During this stage, the oxidation process followed parabolic rate law with high value of rate constant (K_p). On longer exposure of above 15 h, a continuous and more protective scale formed over the surface and further growth of oxide was controlled by diffusion of ions

Table 4 Standard Gibbs free energy of formation of different oxides

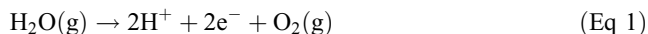
ΔG (in kJ/mole)	Fe_2O_3	Fe_3O_4	Cr_2O_3	FeCr_2O_4	NiO	MnO
ΔG_{600}	- 126.65	- 203.00	- 893.44	- 462.22	- 159.94	- 70.12
ΔG_{650}	- 119.62	- 196.74	- 880.45	- 457.16	- 155.68	- 66.48

through this protective oxide scale; hence, the rate of oxidation was reduced (Table 3). The decrease in the parabolic rate constant (K_p) continued till the scale remained adherent and intact at the surface. The length of the initial oxidation period to form protective oxide layer varies with the chromium content, other alloying additions, partial pressure of oxygen and the oxidation temperature (Ref 9, 10, 32).

During oxidation of an alloy, various types of stress are likely to be generated in the oxide layer due to oxygen dissolution in the metal, volume ratios of oxide to metal, difference in thermal expansion, growth mechanisms of scales and specimen geometry. The stress may cause cracking and spallation of the scales. It reduces the protection by scale and increases the rate of oxidation (Ref 2, 3, 12). During cyclic oxidation of ferrous alloys growth of the oxide scale and thermal stresses are most significant. Thermal stress generates due to the difference in thermal expansion coefficients between the oxide layer and the alloy. As the cyclic oxidation comprises high-temperature heating and cooling to room temperature, thermal stress generates rapidly, which may cause formation of microcracks in the oxide scale. Some cracks may be developed at the oxide/metal interface (Ref 2, 3). Also, stress generates during the growth of the oxide layer. In Fe-Cr alloy, Cr_2O_3 undergoes a phase transformation from pure Cr_2O_3 to a spinel structure, with increase in molar volume, which generates a compressive stress in the scale, as a result of which microcracks are formed in the oxide scale (Ref 12). Through these microcracks, gaseous oxygen comes into direct contact of the chromium depleted region of substrate and iron oxide may form beneath the scale. The scales may fail by cracking if the level of the stress in the oxide scale is high enough. Repetitive thermal stress and continuous growth of the oxide scale may cause propagation of the microcracks into bigger cracks and lead to spallation of the oxide scale (Ref 2, 12). After scale spallation, the bare material again reacts vigorously with oxygen and oxidation occurs at an increased rate until again a protective oxide scale forms over the surface. As the USP process causes severe plastic deformation on the surface by compressive stress, pores, cavity-like defects just beneath the surface are removed (Ref 24). It helps to form a hard and adherent oxide scale and maintains the higher oxidation resistance for longer duration of exposure. On the other hand, the USP process also imparts high amount of residual stress on sample surface, which lowers the oxidation resistance. Sometimes the formation of microcracks in the oxide scale may increase the oxidation rate via gas contamination. Increase of the surface roughness also results in higher oxidation rate of a material. Therefore, an optimum combination of all these factors can improve the total oxidation resistance of a material depending on materials property and oxidation conditions.

3.1.3 Oxidation of the T91 Steel in Steam at 650 °C. It is reported that due to presence of water vapor in the environment, the oxidation rate of Fe-Cr alloys is accelerated

(Ref 9-12, 32). Some researchers proposed that presence of steam in environment changes the diffusion behavior of oxygen in the oxide scale (Ref 9, 10). At higher temperature H_2O dissociates into H^+ ions and O_2 .

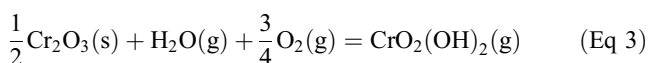


A number of researches show that at high temperatures H^+ might dissolve in metal oxides and forms iron hydroxide, which affect their defect structures. Some oxides may even become highly conductive for ions (Ref 9). Also,

$$K = c(\text{H}^+)^2 \cdot c(\text{e}^-)^2 \cdot p(\text{O}_2)^{1/2} \cdot p(\text{H}_2\text{O})^{-1} \quad (\text{Eq 2})$$

where 'K' is the reaction equilibrium constant and 'p' is the partial pressure of gases. During the steam oxidation experiment, only water vapor was introduced, and the water vapor pressure was set constant. According to the above Eq 2, partial pressure of oxygen and the concentration of H^+ ions are inversely related to each other. Therefore, more hydrogen defects in the oxide layer accelerate ion diffusion in the oxide layer. On the other hand, higher partial pressure of O_2 accelerates the oxidation reaction. Under both these conditions, the oxidation rate of the substrate steel is accelerated in water vapor environment (Ref 9, 11).

Still others proposed that steam causes transformation of protective Cr-rich oxide into non-protective Fe-rich oxide scales (Ref 29, 32, 34). Above 600 °C H_2O in presence of oxygen reacts with Cr_2O_3 and produces volatile $\text{CrO}_2(\text{OH})_2$ as per the following reaction (Eq 3).



Though the rate of this reaction is slow at 650 °C, continuous volatilization/evaporation of Cr_2O_3 results in loss of Cr_2O_3 from the oxide scale and gradually the oxide becomes Fe-rich (Ref 32, 34). If the overall Cr concentration comes below a critical level, the protectiveness of the oxide layer decreases and rate of oxidation increases rapidly. To prevent this increased oxidation, it is necessary to maintain the continuous supply of Cr enhancing its diffusion rate from substrate to the oxidizing surface (Ref 29).

The variation of weight gain per unit area (ΔW) with exposure time in oxidation of the T91 steel in steam at 650 °C for 48 h is shown in Fig. 8(a). In this case also, initially weight gain rate is very high for the first 20 h, after that the weight gain rate decreased. As the 'n' value was nearly 2 in the initial stages of oxidation in steam, it is assumed that oxidation kinetics followed nearly parabolic rate law. From the $(\Delta W)^2$ versus exposure time plot (Fig. 8b), the values of ' K_p ' were determined at different time intervals and are listed in Table 5. It can be seen that the total weight gain is higher in steam than that from oxidation in air, that implies higher oxidation rate in steam. The formation and volatilization of $\text{CrO}_2(\text{OH})_2$ may cause some weight loss, but due to decrease of oxidation resistance, iron

oxidized more and the total weight gain (ΔW) is higher than in air oxidation. The oxidation rate in steam was decreased for all the USP treated specimens in respect of the Un-USP specimen. It suggests that enhanced diffusivity of Cr in the USP treated samples helped in compensating the loss of Cr from oxidizing surface. Thus the deleterious effect of steam environment was overcome and oxidation resistance was increased in USP-treated condition. Highest weight gain was observed for the Un-USP sample, and it was lowest for the USP2.0 specimen. The optical micrographs of cross sections of the Un-USP and USP-treated samples of T91 steel after 48 h of oxidation in steam at 650 °C show a thick oxide layer over the surface (Fig. 9). For the Un-USP sample, the oxide scale formed was

non-uniform. A clear oxide-metal interface can be seen in the micrographs. A different USP-modified region of 300-350 μm can also be seen in the micrograph of the USP-treated samples, and the thickness of these layers increased with increase in USP time duration.

The SEM micrographs of the Un-USP and USP2.0 T91 steel samples oxidized in steam show clearly that a thick oxide layer has formed over the surface (Fig. 10). The oxide layer for the Un-USP sample is much thicker (140-150 μm) than that formed over the USP2.0 specimen (70-80 μm). The oxide layer is rough for the Un-USP sample, and the oxide layer of USP2.0 is relatively smoother. The EDS analysis of the oxide scales in cross section of the oxidized specimens in Fig. 10 show that outer layer of the oxide scales consist of only iron and oxygen, like that formed from oxidation in air. No chromium was found in outer oxide layer of the Un-USP sample. In the USP2.0 sample, some amount of Cr was present at the outer scale and amount of Cr was higher in the inner scale as compared to that in the Un-USP sample. The inner oxide layer consists of both iron and chromium oxide. Some amounts of Mo and Mn were also present in the oxide scale of the USP2.0 sample. The amount of oxygen in the oxide scale had decreased in the USP2.0 sample, which reflects higher oxidation resistance of the USP2.0 specimen.

The XRD patterns of the oxide scale formed from the oxidation of the Un-USP and different USP-treated samples in steam for 48 h are shown in Fig. 11. Analysis of the XRD data shows different types of oxides formed during the steam oxidation test. All the oxide scales contain various ferrous and chromium oxides like Fe_2O_3 , FeO , Fe_3O_4 , Cr_2O_3 and FeCr_2O_4 . The major compound was found to be Fe_2O_3 . For the Un-USP sample, the intensity of almost all the peaks are highest and for the USP2.0 sample the intensities are lowest. It means that the thickness of the oxide layer was highest for the Un-USP sample and was lowest for the USP2.0 sample.

3.2 The SS347 Steel Super-Heater Material

The SS347 steel contains austenite grains, with twin bands in many of the grains. The mean intercept length of grains is generally 48-50 μm (Ref 13-15). The average bulk hardness of the as-received SS347 specimen was measured to be 220 ± 5 VHN. Due to presence of carbide particles along the grain boundaries and solid solution strengthening by Ni and Mo, the hardness is high. The carbide particles are M_{26}C (Cr_{26}C) and MC (NbC) types, which strengthen the material and retard grain growth at higher temperature.

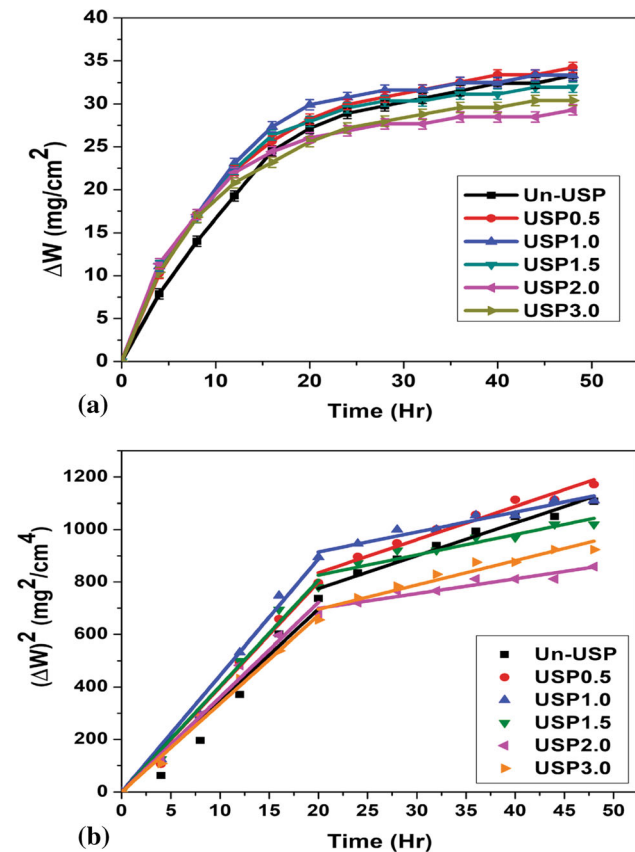


Fig. 8 Variation of (a) ΔW with exposure time, (b) $(\Delta W)^2$ with exposure time of different USP treated T91 steel oxidized in steam at 650 °C for 48 h

Table 5 Data of rate constant of oxidation of Un-USP and different USP treated T91 steel oxidized in steam at 650 °C for 48 h

Sample	$(\Delta W)^2 = K_p t$					
	$n \ln(\Delta W) = \ln(K) + \ln(t)$		Up to 20 h		After 20 h	
	n	adj. R^2	$K_p, \text{mg}^2 \text{cm}^{-4} \text{h}^{-1}$	adj. R^2	$K_p, \text{mg}^2 \text{cm}^{-4} \text{h}^{-1}$	adj. R^2
Un-USP	1.50	0.96	34.82	0.979	12.54	0.959
USP0.5	1.85	0.96	39.97	0.996	12.64	0.958
USP1.0	1.91	0.95	44.39	0.994	7.59	0.943
USP1.5	2.31	0.94	40.33	0.995	7.76	0.885
USP2.0	2.06	0.96	36.09	0.995	5.64	0.901
USP3.0	2.00	0.96	33.63	0.997	9.30	0.917

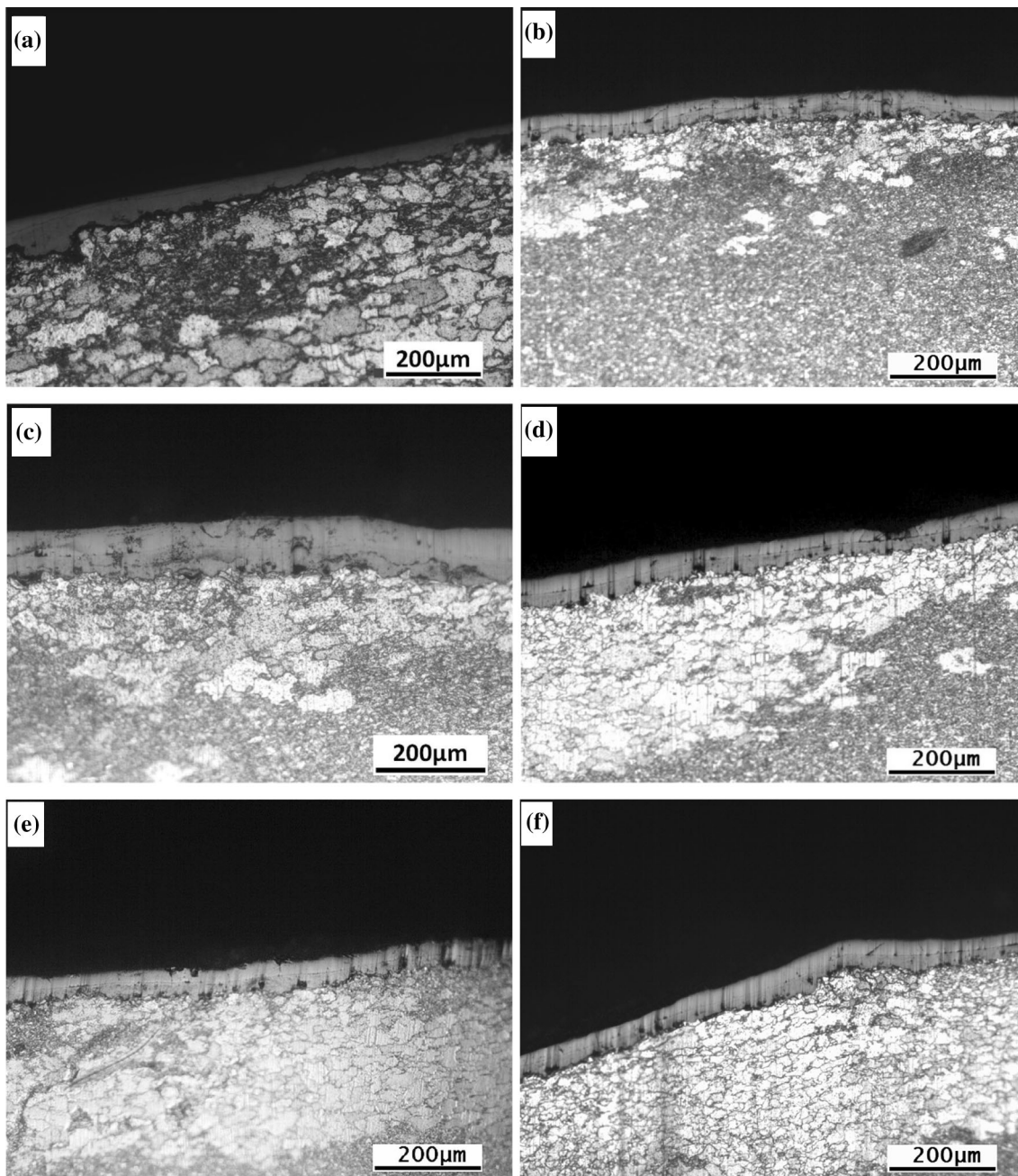


Fig. 9 Optical micrographs of the USP treated T91 steel oxidized in steam at 650 °C for 48 h (a)Un-USP, (b) USP0.5, (c) USP1.0, (d) USP1.5, (e) USP2.0, and (f) USP3.0

3.2.1 Effect of Ultrasonic Shot Peening. The variation of surface roughness of the SS347 steel with USP time duration is shown in Table 2. The surface roughness of the USP-treated specimens is higher than that of the Un-USP-polished specimen. There is also rapid enhancement in the roughness with the USP time duration up to the USP of 1.5 min.

The hardness of the as-received SS347 steel was found to be 220 ± 5 VHN. Due to USP, the severe plastic deformation process, dislocation density increased at the modified surface layer and the material became harder. The Vickers microhardness values of the USP treated samples are presented in Table 2. It can be seen that USP process enhanced the microhardness by 65% of the USP0.5 and 90% of the USP3.0 at a depth of 50 μm from the USP-treated surface,

and the degree of hardening and the depth of hardened layer increased with the USP time period.

The XRD plots of the Un-USP, USP0.5 and USP3.0 SS347 samples revealed that all the SS347 steel samples had an austenite FCC crystal structure (Fig. 12). The FCC crystal structure of the USP3.0 sample confirms that, in this case also there was no change in the phase of this steel due to the USP treatment. For this steel, the small increment of intensity of the (111), (200) planes are observed, while the intensity of (220) and (311) planes have decreased for the USP-treated samples. For FCC crystal, the (111) plane has highest planar atomic density and lowest CRSS, while the (220) or (311) planes have lower planar atomic density. So, during USP treatment the some of the planes rearranged themselves in the preferred slip

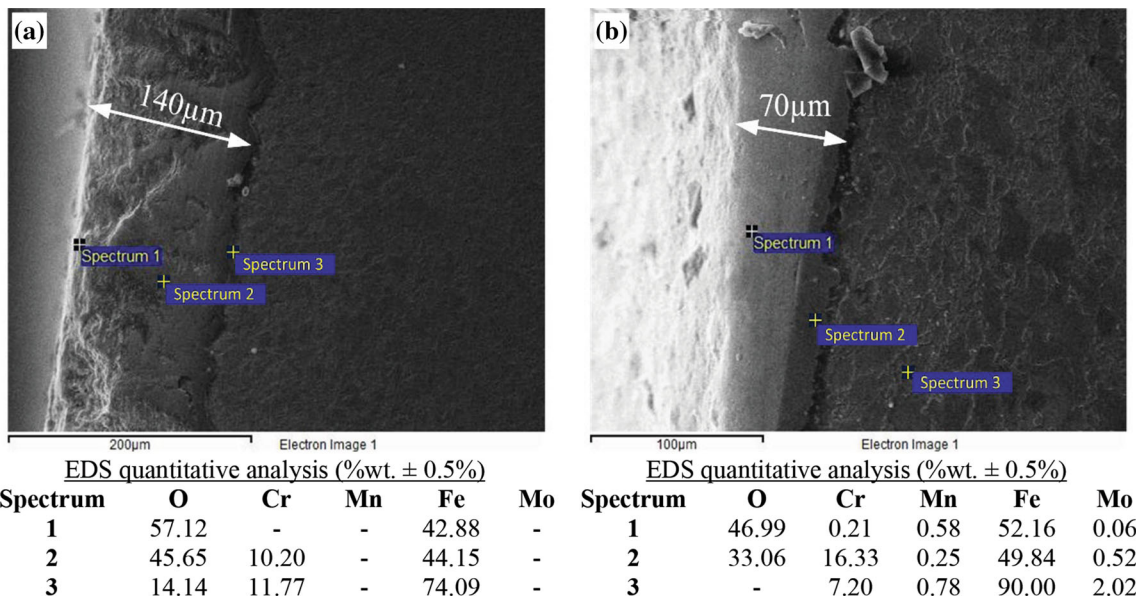


Fig. 10 SEM micrographs and EDS data of the (a) Un-USP, (b) USP2.0 T91 steel oxidized in steam at 650 °C for 48 h

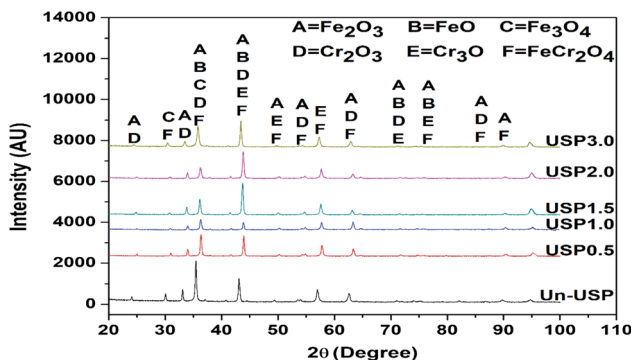


Fig. 11 XRD patterns of the USP treated T91 steel oxidized in steam at 650 °C for 48 h

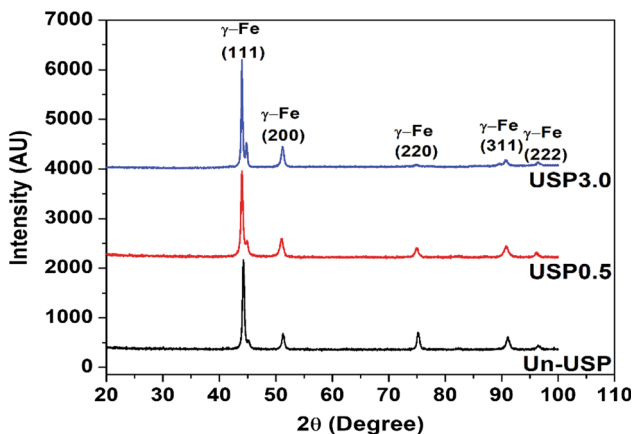


Fig. 12 XRD patterns of the Un-USP, USP0.5 and USP3.0 SS347 steel

plane systems. Though FCC is already a close packed structure, the amount of reorientation of planes is not as much prominent as we can see in less close packed BCC structure.

3.2.2 Oxidation of the SS347 Steel in Air at 650 °C. The exposure of the SS347 austenitic steel at higher temperature shows significantly slower mass gain than that of the T91 steel, which indicates that SS347 steel is very much oxidation resistant than the T91 steel at 650 °C. The variation of weight gain per unit area (ΔW) with exposure time and that of $(\Delta W)^2$ with time for some samples of the SS347 steel during oxidation in air at 650 °C for 68 h are shown in Fig. 13(a) and (b), respectively. Since the sensitivity of the measuring balance was 1 mg and there was very less weight change, the weight gain could not be recorded for even long durations of exposure; hence, hardly 2 readings of weight change could be taken during the entire exposure. Because of this, there was large deviation in data points for the evaluation of 'n' and R^2 values were low. It is evident from the values of 'n' (Table 6) that a near parabolic rate law was followed. For some of the samples, weight gain was extremely low; hence, $(\Delta W)^2$ versus time plot could not be established properly. The analyzed ' K_p ' and R^2 values are listed in Table 6. The oxidation rate was decreased only for the USP2.0 and USP3.0 specimens, but it was increased for the other USP-treated specimens. There was highest oxidation rate of the USP1.0 sample and lowest of the USP3.0.

In the initial stage of oxidation of austenitic steels, a thin protective scale of Cr_2O_3 oxide is formed on the alloy steel. At higher partial pressures of oxygen and higher temperature, along with the Fe_2O_3 and Cr_2O_3 , NiO is also stable according to thermodynamic data (Table 4). At the lower partial pressure, a mixture of several Fe-Ni, Fe-Cr or Fe-Ni-Cr mixed oxides is formed in Ni-containing alloy steel. The oxide scales formed on these commercial Fe-Ni-Cr-based austenitic steels generally consist of spinel, with general formula $M^1M_2^2O_4$, where M^1 is Fe, Ni or Mn, M^2 is Fe or Cr, and some other oxides of the formula M_2O_3 where $M=Fe, Cr$ or Mn (Ref 13-15, 27, 29). Several researchers have shown that the inner layers of the scales contain these spinel oxides, rich in Fe, Ni and Cr, while the outer layers are rich only in Fe (Ref 1, 13, 33). Another proposed mechanism for the growth of scale on Ni-Cr steels is that the initially formed Cr_2O_3 layer was a p-type semicon-

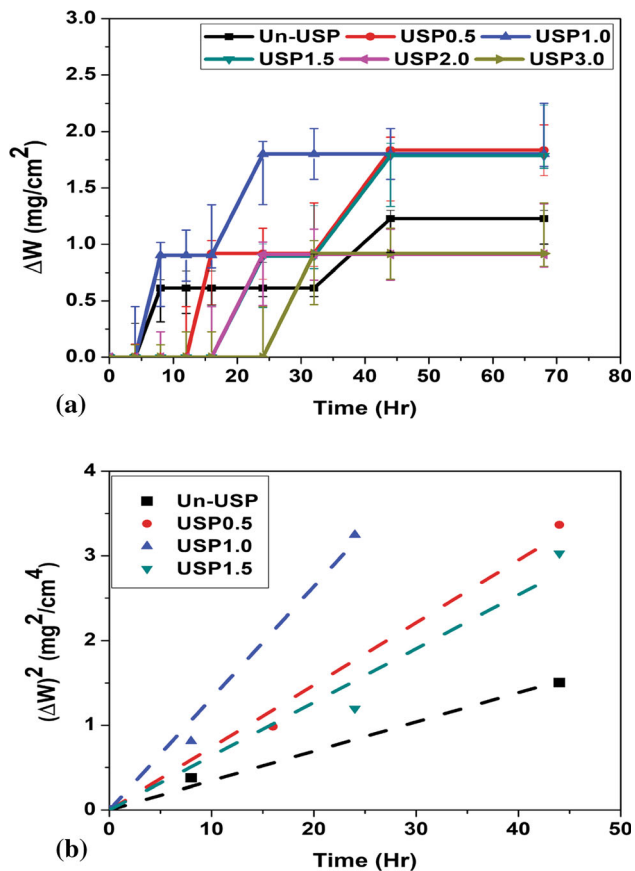


Fig. 13 Variation of (a) ΔW with exposure time, (b) $(\Delta W)^2$ with exposure time of the different USP-treated SS347 steel oxidized in air at 650 °C for 68 h. The plots in (b) are shown by dashed lines because of only 2 available data points

Table 6 Data of rate constant of oxidation of Un-USP and different USP-treated SS347 steel oxidized in air at 650 °C for 68 h

Sample	$n \cdot \ln(\Delta W) = \ln(K) + \ln(t)$		$(\Delta W)^2 = K_p \cdot t$	
	n	adj. R^2	K_p , $\text{mg}^2 \text{cm}^{-4} \text{h}^{-1}$	adj. R^2
Un-USP	1.82	0.77	0.0346	0.994
USP0.5	1.71	0.76	0.0737	0.984
USP1.0	1.33	0.75	0.1319	0.991
USP1.5	1.58	0.77	0.0635	0.905
USP2.0	1.38	0.72	0.0344	0.999
USP3.0	1.42	0.74	0.0263	0.999

ductor which grew by cation diffusion. Fe^{2+} and Ni^{2+} ions tend to reduce the number of cation vacancies per unit volume of Cr_2O_3 and decrease the oxidation rate (Ref 14, 15). Manganese oxide is also soluble in Cr_2O_3 . If the amount of Mn is sufficient enough, Mn^{4+} ions diffuse rapidly through the Cr_2O_3 via lattice sites, and a Cr-rich Cr-Mn spinel oxide may be formed (Ref 13, 29, 33). Formation of microcracks, voids, porosity accelerates the process. At this stage, the oxidation rate increases rapidly and continues until a protective oxide layer forms again beneath the external scale layers.

From the SEM images of the Un-USP and USP3.0 SS347 steel samples (Fig. 14), it can be seen that a very thin oxide layer formed over the Un-USP and the USP3.0 samples from 68 h of oxidation in air. The scales formed were so thin for all the samples that they could not be revealed by optical microscope. The thickness of the oxide layer is nearly 4–5 μm for the Un-USP sample. The oxide-metal interface is clearly visible and uneven in nature. No noticeable oxide layer is visible over the USP3.0 sample, as the oxide layer formed had a thickness less than 2 μm . The EDS analysis of cross sections of the oxidized SS347 samples shows that the thin oxide layer formed over the surface mainly contains Fe, O, Cr and Ni. It implies that the oxide layer consisted of iron oxide, chromium oxide and nickel oxide. Any large-scale Ni enrichment was not observed at the alloy-oxide interface as the amount of Fe is much higher than that of Ni. Hence, iron and to some extent nickel enter the scale by chemical solution in the Cr_2O_3 and transport along the lattice site, to form outer layers of iron-nickel-rich oxides. For the USP3.0 sample, no proper oxide scale was found to be characterized. Although the EDS data for the surface of the USP3.0 specimen shows that the amount of Cr in the oxide scale was higher than that of the Un-USP sample; thus, on the USP3.0 specimen more protective chromium oxide layer was formed, and it had better oxidation resistance. The amount of O and Fe is higher in the oxide layer formed on the Un-USP sample; thus, more amount of iron oxide is present in the scale, and it is less oxidation resistant. Also the amount of Cr was higher at a depth of 10–15 μm for the USP3.0 sample than that of the Un-USP specimen.

The XRD patterns of the oxide scale formed from oxidation in air for 68 h of the Un-USP and different USP-treated samples are shown in Fig. 15. It can be seen that various oxides of iron, chromium and nickel formed during the oxidation. As a major oxide product, Fe_2O_3 was present in all the samples. Other oxides like Cr_2O_3 , NiO, FeCr_2O_4 and NiCr_2O_4 were also present on the oxidized surface. As the thickness of the oxide layers was very less, there were peaks of the base material containing austenitic FCC structure. The thickness of the oxide layer formed on the USP3.0 specimen was lowest; thus, there was low intensity of the oxide peaks and high intensity of austenite peaks. However, a reverse trend was observed in case of the USP0.5, USP1.0 and USP1.5 specimens. The intensities of oxide peaks were higher, which implies higher oxidation rate of these specimens.

The high amount of Cr and presence of Ni in the SS347 steel provides excellent oxidation resistance at 650 °C. The USP process should further improve the oxidation resistance by refining grains and increasing diffusion of alloying elements to oxidation surface. However, USP0.5, USP1.0 and USP1.5 samples of SS347 steel show deterioration in their oxidation property. This could be due to the synergistic effect of surface roughness, compressive residual stress and grain refinement on oxidation resistance. Unlike compressive residual stress, the high surface roughness decreases the oxidation resistance. It may be the high surface roughness with inadequate compressive residual stress and grain refinement causes reduction of oxidation resistance for those samples. On the other hand, the negative effect of surface roughness on oxidation resistance was nullified by sufficient amount of compressive residual stress and fine-grained structure at surface for USP2.0 and USP3.0 samples. This negative effect of USP on oxidation resistance is not quite understood and may be associated with non-uniformity of the Cr_2O_3 layer forming on the surface. It

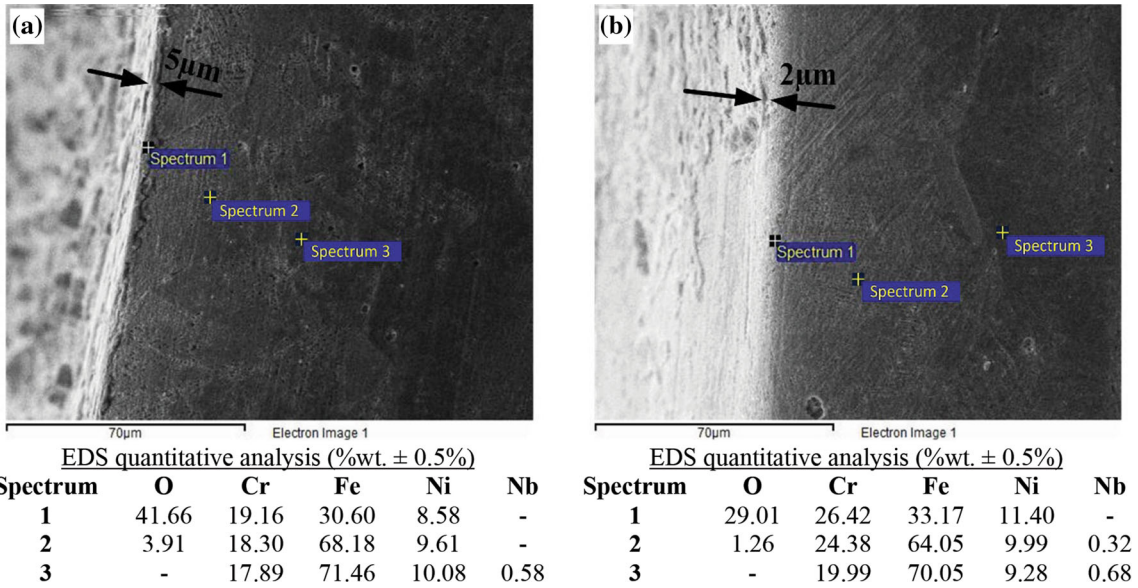


Fig. 14 SEM micrographs and EDS data of the (a) Un-USP, (b) USP3.0 SS347 steel oxidized in air at 650 °C for 68 h

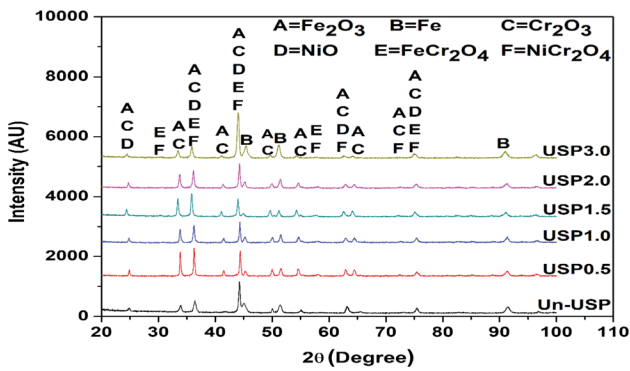


Fig. 15 XRD patterns of the Un-USP and different USP-treated SS347 steel oxidized in air at 650 °C for 68 h

requires further systematic investigation using a much more sensitive weighing balance as the weight gain was extremely low.

3.2.3 Oxidation of the SS347 Steel in Steam at 650 °C. Figure 16(a) shows the variation of weight gain per unit area (ΔW) with exposure time for oxidation of the SS347 steel in steam at 650 °C for 48 h and Fig. 16(b) shows the $(\Delta W)^2$ versus exposure time plot for some of the samples. In this case, also weight gain rate was very low for all the samples. Though steam atmosphere should accelerate the oxidation rate, this steel seems to be highly protective against oxidation at this temperature. Near-parabolic oxidation kinetics was observed for most of the samples; the 'n' and 'K_p' values are listed in Table 7. The steam oxidation rates were less for the USP1.0, USP1.5, USP2.0 and USP3.0 specimens than for the Un-USP specimen. However, USP0.5 sample showed higher oxidation rate than the Un-USP sample. Highest oxidation rate was measured for the USP0.5 sample and lowest oxidation rate was for the USP2.0 specimen.

As the steam oxidation rate for the SS347 steel at 650 °C was very less and the oxide layer formed was very thin, oxide layers were not revealed by optical microscope. From the SEM

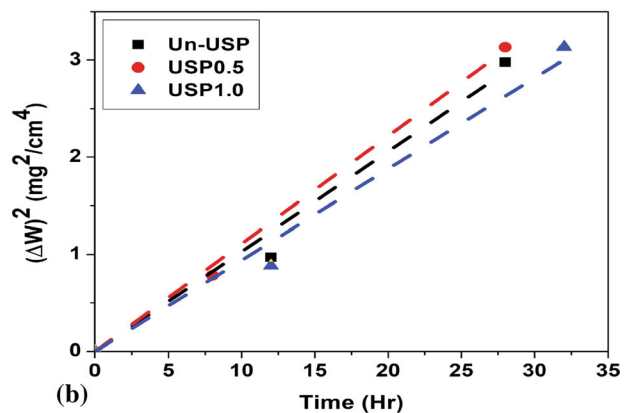
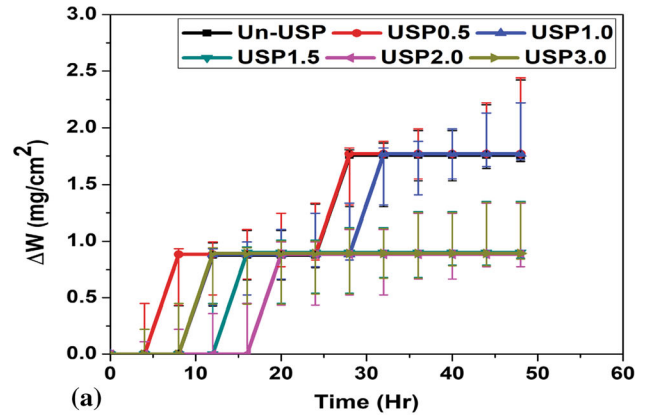


Fig. 16 Variation of (a) ΔW with exposure time, (b) $(\Delta W)^2$ with exposure time of the different USP treated SS347 steel oxidized in steam at 650 °C for 48 h. The plots in (b) are shown by dashed lines because of only 2 available data points

micrographs (Fig. 17) of the Un-USP and the USP2.0 samples of the SS347 steel, oxidized in steam at 650 °C for 48 h, it is evident that very thin oxide layer formed over the surface from oxidation in steam. For the Un-USP sample, the oxide layer is thicker than that of the USP2.0 sample. Thickness of the oxide

layer of the Un-USP sample is 8-10 μm and that of the USP2.0 sample is 4-5 μm . No clear oxide-metal interface was visible for the Un-USP sample, but a clear oxide-metal interface can be seen for the USP2.0 sample. EDS analysis of cross section of the oxide layer of the oxidized samples shows that the thin oxide layers formed over the material surface consist of Fe, Cr, Ni and O. The oxides formed during steam oxidation were of iron, chromium and nickel. The amount of Cr is higher for the USP2.0 sample than that of the Un-USP. Ni amount decreased at the surface for the USP2.0 sample, so less amount of nickel oxide formed during oxidation. The XRD patterns of the oxide scale formed from oxidation of the Un-USP and different USP-treated SS347 samples in steam for 48 h, are shown in Fig. 18. All the scales contain various oxides such as Fe_2O_3 , Fe_3O_4 , Cr_2O_3 , NiO, FeCr_2O_4 and NiCr_2O_4 . As the oxide scale was very thin, peaks of the base material $\gamma\text{-Fe}$ also appeared in the XRD pattern.

In presence of steam the rate of oxidation increased. The combined effect of H^+ ions and higher partial pressure of oxygen accelerated the oxidation kinetics for this steel. The adequate amount of Cr and Ni in SS347 steel helped to form a protective oxide scale containing Cr_2O_3 , NiO and NiCr_2O_4 over the surface. This continuous protective layer over the steel surface retarded the outward movement of metal ions or inward

movement of H^+ and O^{2-} ions. Further, USP process improved the oxidation resistance. However, the adverse effect of USP on oxidation resistance could be seen in USP0.5 sample. This may be attributed to high surface roughness in respect to the grain refinement, which caused an increment of oxidation rate. Therefore, optimization of grain refinement, compressive residual stress and surface roughness is required to obtain the best oxidation resistance.

4. Comparison of USP Effect on Oxidation Behavior of T91 and SS347 Steels

To get good oxidation resistance in a steel, minimum 10-12 wt.% of Cr is essential which can form a continuous protective Cr_2O_3 scale over the surface. In case of the T91 steel, the nominal content of Cr is about 9 wt.%, which is not sufficient to provide a good oxidation resistance. Due to the USP treatment, the diffusion rate of Cr from the bulk to the surface region is increased at elevated temperature. Figure 19 schematically shows the mechanism of oxidation process in the USP-treated

Table 7 Data of rate constant of oxidation of Un-USP and different USP-treated SS347 steel oxidized in steam at 650 °C for 48 h

Sample	$n \cdot \ln(\Delta W) = \ln(K) + \ln(t)$		$(\Delta W)^2 = K_p \cdot t$	
	<i>n</i>	adj. <i>R</i> ²	<i>K_p</i> , $\text{mg}^2 \text{cm}^{-4} \text{h}^{-1}$	adj. <i>R</i> ²
Un-USP	1.75	0.78	0.1028	0.962
USP0.5	1.77	0.80	0.1108	0.998
USP1.0	1.71	0.78	0.0939	0.981
USP1.5	1.42	0.74	0.0507	0.999
USP2.0	1.52	0.76	0.0392	0.999
USP3.0	1.48	0.72	0.0664	0.999

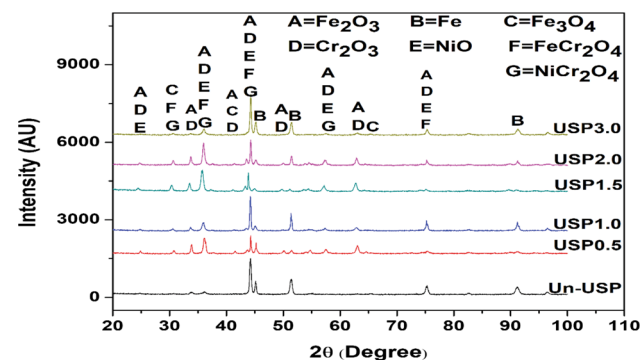
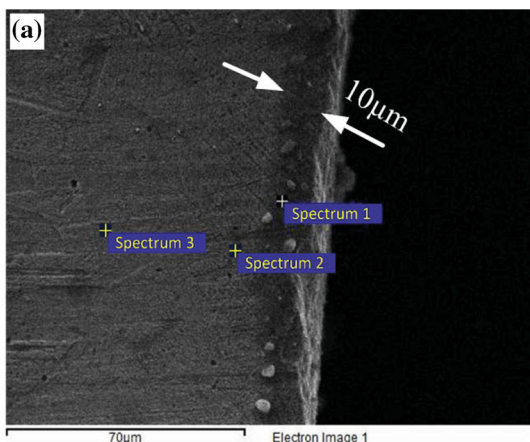
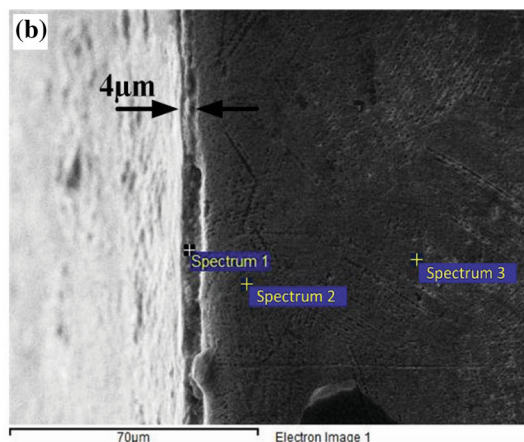


Fig. 18 XRD patterns of the different USP treated SS347 steel oxidized in steam at 650 °C for 48 h



EDS quantitative analysis (%wt. $\pm 0.5\%$)

Spectrum	O	Cr	Fe	Ni	Nb
1	42.16	16.74	31.78	9.32	-
2	2.17	17.74	68.78	11.32	-
3	-	17.43	71.31	10.65	0.62



EDS quantitative analysis (%wt. $\pm 0.5\%$)

Spectrum	O	Cr	Fe	Ni	Nb
1	39.85	25.63	26.12	8.40	-
2	1.20	22.52	66.26	10.02	-
3	-	20.09	68.73	10.48	0.70

Fig. 17 SEM micrographs and EDS data of the (a) Un-USP, (b) USP2.0 SS347 steel oxidized in steam at 650 °C for 48 h

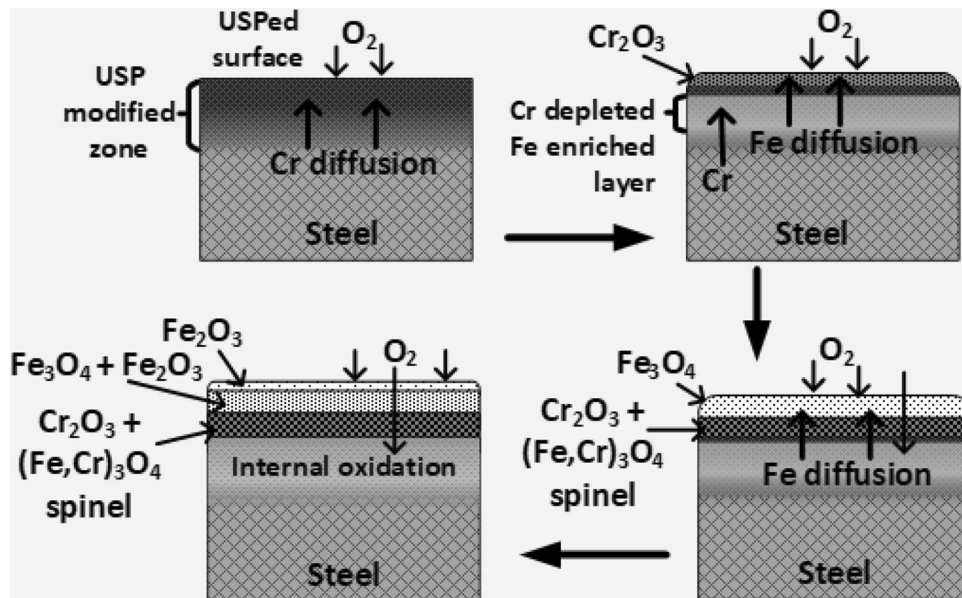


Fig. 19 Schematic diagram showing effect of USP on oxidation process of the T91 steel at 650 °C

T91 steel at 650 °C. In the surface region, Cr content increases while a Cr-depleted region forms just beneath the USP-affected layer. Cr content in the Cr-depleted region did not fall below a critical level due to diffusion from the bulk, below the Cr-depleted zone. Hence, not much internal oxidation of Fe occurred in the Cr depleted region and oxidation resistance was maintained during the period of exposure. Thus, the positive effect of USP in improving the oxidation resistance was more pronounced on the T91 steel in both air and steam oxidation at 650 °C.

On the other hand, the SS347 steel contained about 18 wt.% of Cr along with 10 wt.% of Ni, which is higher than the critical amount required to get a good oxidation resistance. For both the Un-USP and USP specimens of SS347 steel, the weight gain was very less. The maximum mass gain was only 1.8 and 1.7 mg/cm² from exposure in air and steam, respectively, for this steel, whereas for the T91 steel it was 27.3 and 34.2 mg/cm² from exposure in air and steam, respectively. Because of the very less weight change, it is evident that SS347 steel has inherently high oxidation resistance at 650 °C. As this steel already has very high oxidation resistance at 650 °C both in air and steam environment, the effect of USP was not clearly observed for this steel at this temperature.

5. Conclusions

The effect of ultrasonic shot peening on surface modification and oxidation behavior in air and steam at 650 °C was studied for the T91 and the SS347 steels, and the following conclusions are drawn:

- Surface morphology and other surface properties were modified by USP treatment. The USP process increased surface roughness of both the steels, and the surface roughness increased with USP time duration. USP process also enhanced the microhardness of the T91 steel by 51% for the 30 s USP-treated sample at a depth of 50 μm from

the USP-treated edge. For the SS347 steel, the microhardness was increased up to 65% at a depth of 60 μm from the USP-treated edge through USP treatment of 30 s. The degree of hardening and the depth of hardened layer increased with USP time period.

- The USP process did not cause any phase transformation either for the T91 steel or for the SS347 steel. However, a little texture was observed on (110) planes for the T91 steel and on (111) planes for the SS347 steel. The (110) and (111) planes are the most preferable slip planes in BCC and FCC crystal structure, respectively.
- High-temperature oxidation resistance of the T91 steel in air and steam at 650 °C was improved by the USP. The amount of Cr and other alloying elements in the oxide scale was higher in the USP-treated specimens than that in the Un-USP specimen, due to higher diffusion rate of the alloying elements to surface during high-temperature exposure. Hence, the oxide scales were more protective to oxidation. However, induced residual stress in USPed surface and gas contamination through microcracks also affect the oxidation resistance. An optimum combination of all these factors gives improved oxidation resistance of an USPed material. Lowest oxidation rate of the T91 steel in air was observed for the USP1.5 sample. Highest oxidation resistance in steam environment was observed for the USP2.0 specimen.
- The oxidation resistance of the SS347 at 650 °C in both air as well as in steam was high enough to show any significant change in mass gain. The increase in weight gain per unit area (ΔW) in the SS347 steel in the Un-USP condition was extremely low. Therefore, the USP had only insignificant effect in improving the oxidation resistance. However, the oxidation resistance of the SS347 steel in air at 650 °C was improved for the USP2.0 and USP3.0 samples but was reduced for the USP0.5, USP1.0 and USP1.5 samples. Highest oxidation resistance in air was for the USP3.0 specimen. The oxidation resistance in steam at 650 °C for the SS347 steel was improved for the USP treated specimens and highest oxidation resistance

was for the USP2.0 sample.

- The thickness of the oxide scale formed during high-temperature oxidation decreased with increase in the USP time duration. Exfoliation tendency of the oxide scale also decreased for the T91 steel with increase in the time period of USP.

Acknowledgments

The authors would like to express their gratitude for the help from Mr. Rohit Shukla for providing the material for this work.

References

1. T. Dudziak, M. Lukaszewicz, N. Simms, and J. Nicholls, Analysis of High Temperature Steam Oxidation of Superheater Steels Used in Coal Fired Boilers, *Oxid. Met.*, 2016, **85**, p 171–187
2. R. Viswanathan and W. Bakker, Materials for Ultrasupercritical Coal Power Plants-Boiler Materials: Part 1, *J. Mater. Eng. Perform.*, 2001, **10**(1), p 81–95
3. R.Y. Chen and W.Y.D. Yeun, Review of the High-Temperature Oxidation of Iron and Carbon Steels in Air and Oxygen, *Oxid. Met.*, 2003, **59**, p 433–468
4. A. Fry, S. Osgerby, M. Wright, Oxidation of Alloys in Steam Environments. NPL Report MATC(A)90 (2002)
5. J.P.T. Vossen, P. Gawenda, K. Rahts, M. Röhrig, M. Schorr, and M. Schütze, Limits of the Oxidation Resistance of Several Heat-Resistant Steels Under Isothermal and Cyclic Oxidation as Well as Under Creep in Air at 650 °C, *Mater. High Temp.*, 1997, **14**(4), p 387–401
6. R.L. Klueh and A.T. Nelson, Ferritic/Martensitic Steels for Next-Generation Reactors, *J. Nucl. Mater.*, 2007, **371**(1), p 37–52
7. J. Hald, Metallurgy and Creep Properties of New 9-12%Cr Steels, *Steel Res.*, 1996, **67**(9), p 369–374
8. K. Anish, Characterisation of Microstructure in 9% Chromium Ferritic Steels Using Ultrasonic Measurements, *Trans. Indian Inst. Met.*, 2003, **56**(5), p 483–497
9. Z. Du-qing, L. Guang-ming, Z. Guo-qun, and G. Yan-jin, Cyclic Oxidation Behavior of Fe-9Cr-1Mo Steel in Water Vapor Atmosphere, *J. Central South Univ. Technol.*, 2009, **16**(4), p 535–540
10. D. Laverde, G. Acebo, and F. Castro, Continuous and Cyclic Oxidation of T91 Ferritic Steel Under Steam, *Corros. Sci.*, 2004, **46**, p 613–631
11. P.J. Ennis and W.J. Quadackers, Mechanisms of Steam Oxidation in High Strength Martensitic Steels, *Int. J. Press. Vessels Pip.*, 2007, **84**, p 75–81
12. F. Eberle and C.H. Anderson, Scaling Behaviour of Superheater Tube Alloys in ASME High-Temperature Steam Research Tests at 1100-1500F, *J. Eng. Power*, 1962, **84**(3), p 223–257
13. Y. Li, S. Wang, P. Sun, D. Xu, M. Ren, Y. Guo, and G. Lin, Early Oxidation Mechanism of Austenitic Stainless Steel TP347H in Supercritical Water, *Corros. Sci.*, 2017, **128**, p 241–252
14. H. Viitala, I. Galfi, and P. Taskinen, Initial Oxidation Behaviour of Niobium Stabilized TP347H Austenitic Stainless Steel—Effect of Grain Size and Temperature, *Mater. Corros.*, 2015, **66**(9), p 851–862
15. Z. Liang and Q. Zhao, Steam Oxidation of Austenitic Heat-Resistant Steels TP347H and TP347HFG at 650-800 °C, *Materials*, 2019, **12**, p 577–592
16. F. Abe and M. Tabuchi, Microstructure and Creep Strength of Welds in Advanced Ferritic Power Plant Steels, *Sci. Technol. Weld. Join.*, 2004, **9**(1), p 22–30
17. S. Jelliti, C. Richard, D. Retraint, T. Roland, M. Chemkhi, and C. Demangel, Effect of Surface Nanocrystallization on the Corrosion Behavior of Ti-6Al-4 V Titanium Alloy, *Surf. Coat. Technol.*, 2013, **224**, p 82–87
18. X.Y. Wang and D.Y. Li, Mechanical and Electrochemical Behavior of Nanocrystalline Surface of 304 stainless Steel, *Electrochim. Acta*, 2002, **47**, p 3939–3947
19. K.S. Raja, S.A. Namjoshi, and M. Misra, Improved Corrosion Resistance of Ni-22Cr-13Mo-4 W Alloy by Surface Nanocrystallization, *Mater. Lett.*, 2005, **59**, p 570–574
20. T. Balusamy, S. Kumar, and T.S. Narayanan, Effect of Surface Nanocrystallization on the Corrosion Behaviour of AISI, 409 Stainless Steel, *Corros. Sci.*, 2010, **52**(11), p 3826–3834
21. M. Malaki and H. Ding, A Review of Ultrasonic Peening Treatment, *Mater. Des.*, 2015, **87**, p 1072–1086
22. H. Kumar, S. Singh, and P. Kumar, Modified Shot Peening Processes, *Int. J. Eng. Sci. Emerg. Technol.*, 2013, **5**(1), p 12–19
23. T. Roland, Enhanced Mechanical Behavior of a Nanocrystallised Stainless Steel and Its Thermal Stability, *Mater. Sci. Eng. (A)*, 2007, **445–446**, p 281–288
24. G.J. Gibson, K.M. Perkins, S. Gray, and A.J. Leggett, Influence of Shot Peening on High-Temperature Corrosion and Corrosion-Fatigue of Nickel Based Superalloy 720Li, *Mater. High Temp.*, 2016, **33**(3), p 225–233
25. D. Bandla, P. Verma, K. Chattopadhyay, and V. Singh, Enhancement of Hot Corrosion Resistance of Modified 9Cr-1Mo Steel Through Surface Nanostructuring and Pre-oxidation, *J. Mater. Eng. Perform.*, 2018, **27**(12), p 6443–6457
26. A.K. Shukla, D. Gondb, M. Bharadwaja, and D. Puria, High Temperature Oxidation and Hot Corrosion Behaviour of 9Cr 1Mo Ferritic Cold Rolled Steel in Air at 900 °C Under Cyclic Condition, *J. Miner. Mater. Charact. Eng.*, 2011, **10**(11), p 1061–1075
27. R. Naraparaju, V.B. Trindade, H.-J. Christ, and U. Krupp, Effect of Shot-Peening on the Oxidation Behaviour of Boiler Steels: Experimental Results and Simulation, *Corros. Eng., Sci. Technol.*, 2009, **44**(3), p 211–217
28. J.S. Peltz, L.V.R. Beltrami, S.R. Kunstb, C. Brandolta, and C.F. Malfattia, Effect of the Shot Peening Process on the Corrosion and Oxidation Resistance of AISI430 Stainless Steel, *Mater. Res.*, 2015, **18**(3), p 538–545
29. X. Peng, Effect of Grain Refinement on the Resistance of 304 Stainless Steel to Breakaway Oxidation in Wet Air, *Acta Mater.*, 2005, **53**, p 5079–5088
30. J. Moering, X. Ma, G. Chen, P. Miao, G. Li, G. Qian, S. Mathaudhu, and Y. Zhu, The Role of Shear Strain on Texture and Microstructural Gradients in Low Carbon Steel Processed by Surface Mechanical Attrition Treatment, *Scripta Materialia*, 2015, **108**, p 100–103
31. M. Ratto, E. Ricci, E. Arato, and P. Costa, Oxidation of Metals with Highly Reactive Vapors: Extension of Wagner theory, *Metall. Mater. Trans. B*, 2001, **32**(5), p 903–911
32. J. Yuan, X. Wu, W. Wang, S. Zhu, and F. Wang, Investigation on the Enhanced Oxidation of Ferritic/Martensitic Steel P92 in Pure Steam, *Materials*, 2014, **7**, p 2772–2783
33. M.K. Singh, S. Kumar, O.P. Sinha, V. Singh, and G.S. Mahobia, Cyclic Oxidation Behavior of the Super Austenitic Stainless Steel 904L in Air at 500-650 °C, *Trans. Indian Inst. Met.*, 2020, **73**(4), p 1101–1108
34. K. Segerdahl, J.E. Svensson, M. Halvarsson, I. Panas, and L.G. Johansson, Breakdown of the Protective Oxide on 11% Cr Steel at High Temperature in the Presence of Water Vapor and Oxygen, the Influence of Chromium Vaporization, *Mater. High Temp.*, 2005, **22**(1), p 69–78

Publisher's Note Springer Nature remains neutral with regard to jurisdictional claims in published maps and institutional affiliations.